Supplementary Information for

Asymmetric Pendrin Homodimer Reveals its Molecular Mechanism as Anion Exchanger

Qianying Liu[1#], Xiang Zhang[1#], Hui Huang[1#], Yuxin Chen[2,5,6,7#], Fang Wang[2,5,6,7], Aihua Hao[1], Wuqiang Zhan[1], Qiyu Mao[1], Yuxia Hu[1], Lin Han[1], Yifang Sun[1], Meng Zhang[1], Zhimin Liu[1], Genglin Li[2], Weijia Zhang[1], Yilai Shu[2,5,6,7*], Lei Sun[1,3,4*], Zhenguo Chen[1,3,4*]

Correspondence to: zhenguochen@fudan.edu.cn (Z.C.); llsun@fudan.edu.cn (L.S.); and yilai_shu@fudan.edu.cn (Y.S.)

This PDF file includes:

Supplementary Fig. 1-12

Supplementary Table 1-3

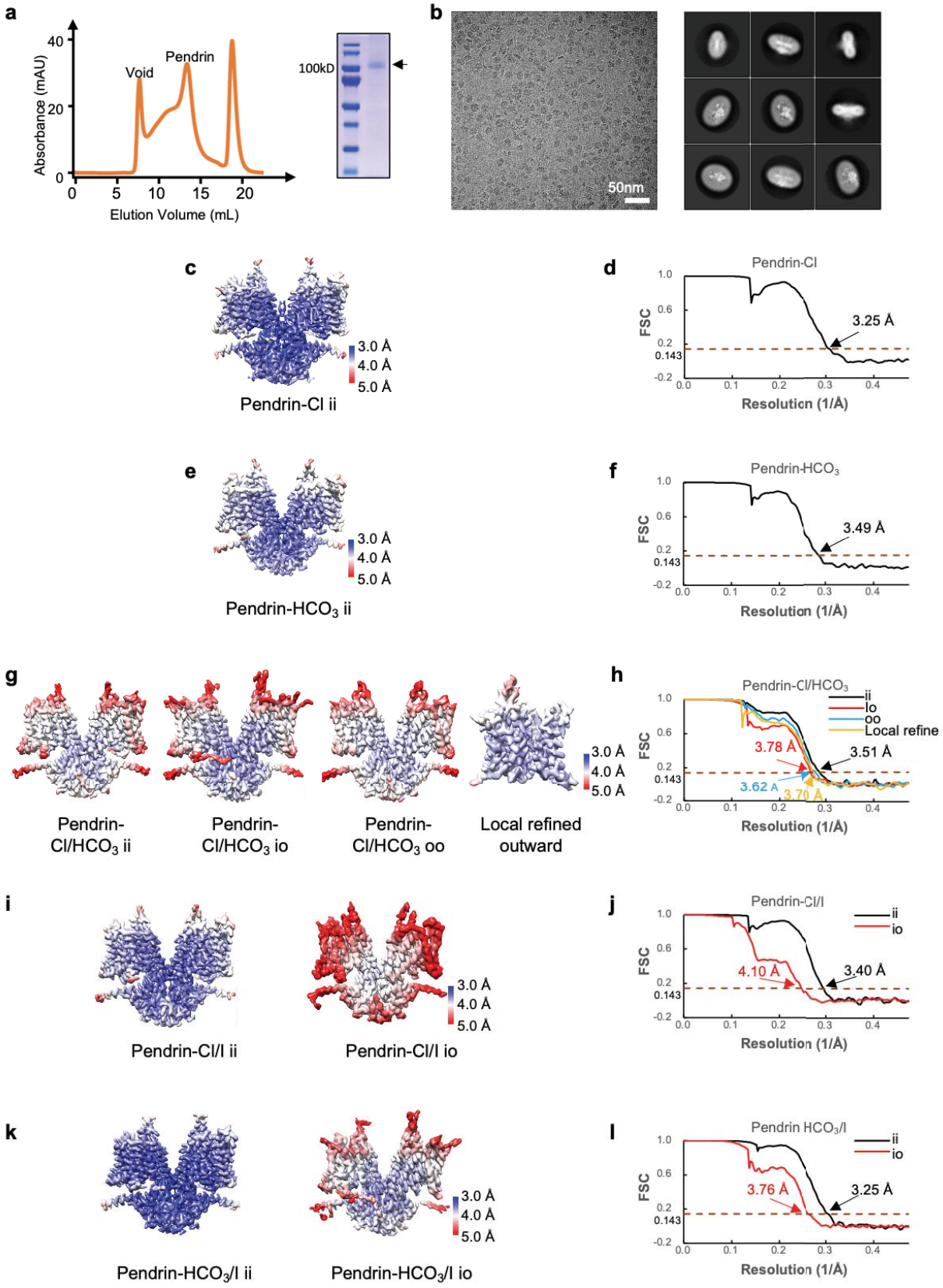
a
Absorbance (mAU)
40
20
0
0
5
10
15
20
Elution Volume (mL)
Void
Pendrin
100kD
b
50nm
c
3.0 Å
4.0 Å
5.0 Å
Pendrin-Cl ii
d
Pendrin-Cl
FSC
1.0
0.6
0.2
0.143
-0.2
0.0
0.1
0.2
0.3
0.4
Resolution (1/Å)
3.25 Å
e
3.0 Å
4.0 Å
5.0 Å
Pendrin-HCO3 ii
f
Pendrin-HCO3
3.49 Å
g
3.0 Å
4.0 Å
5.0 Å
Pendrin-Cl/HCO3 ii
Pendrin-Cl/HCO3 io
Pendrin-Cl/HCO3 oo
Local refined outward
h
Pendrin-Cl/HCO3
ii
Io
oo
Local refine
3.78 Å
3.51 Å
3.62 Å
3.70 Å
i
3.0 Å
4.0 Å
5.0 Å
Pendrin-Cl/I ii
Pendrin-Cl/I io
j
Pendrin-Cl/I
ii
io
4.10 Å
3.40 Å
k
3.0 Å
4.0 Å
5.0 Å
Pendrin-HCO3/I ii
Pendrin-HCO3/I io
l
Pendrin HCO3/I
ii
io
3.76 Å
3.25 Å

Supplementary Fig. 1 Purification and cryo-EM data processing results of pendrin.

a, Size exclusion chromatography of pendrin-Cl and SDS-PAGE gel of the peak fraction. The features and patterns were similar among all five data sets' purification. **b,** The representative of Cryo-EM micrographs and the 2D averages from pendrin-Cl dataset. **c, e, g, i, k,** Cryo-EM maps colored according to local resolution estimations. **d, f, h, j, l,** Corresponding FSC curves of the masked cryo-EM maps. ii: inward-inward, io: inward-outward, oo: outward-outward for protomer A and protomer B, respectively.

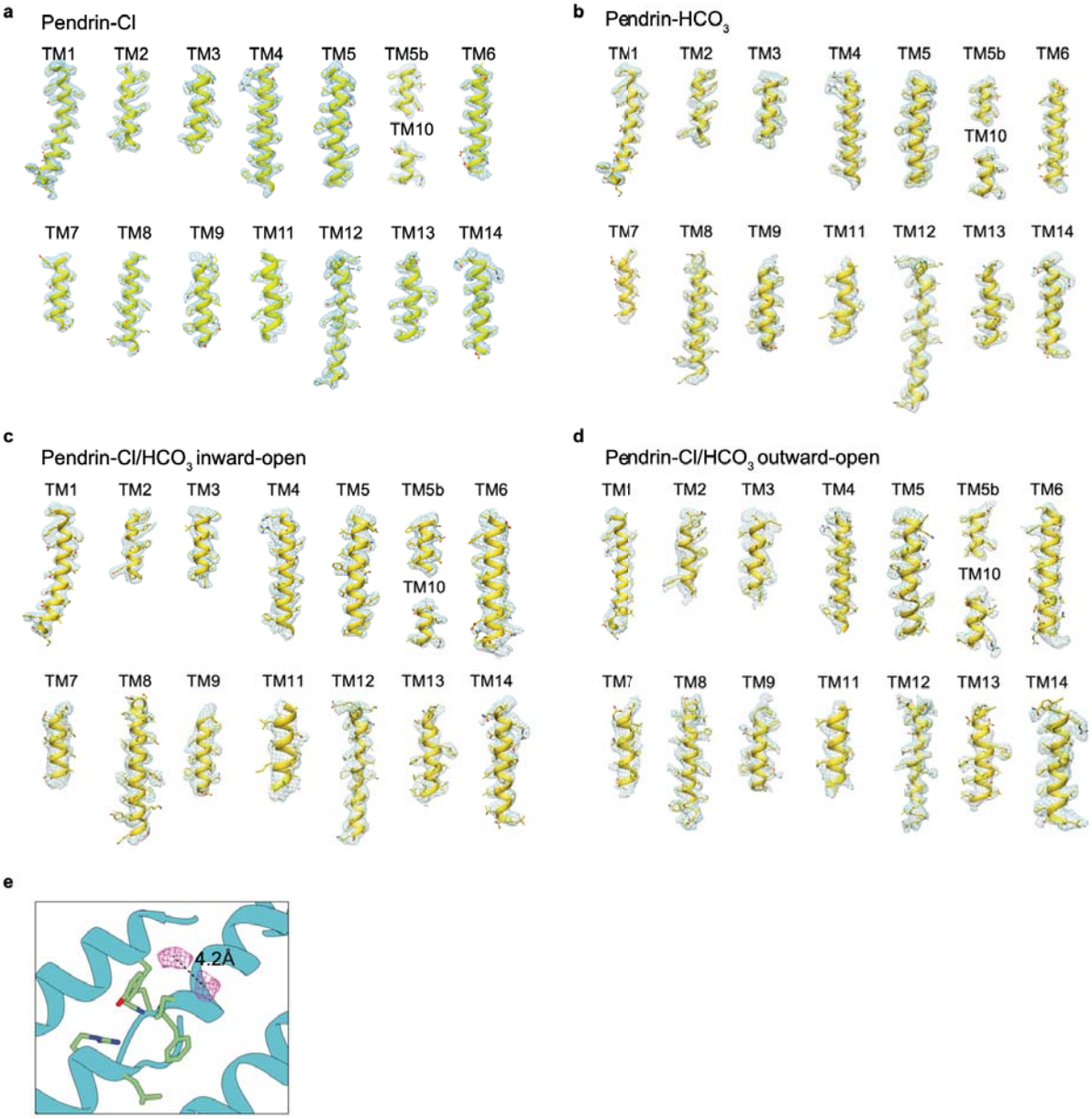

Supplementary Fig. 2 Local cryo-EM densities.

a, Representative local cryo-EM densities of pendrin-Cl $_{ii}$. **b,** Representative local cryo-EM densities of pendrin-$HCO_{3\ ii}$. **c** and **d,** Representative local cryo-EM densities of pendrin-Cl/$HCO_{3\ io}$. **e,** Two anion densities in the outward-open cavity in pendrin-Cl/HCO_3. The distance between two densities is labeled.

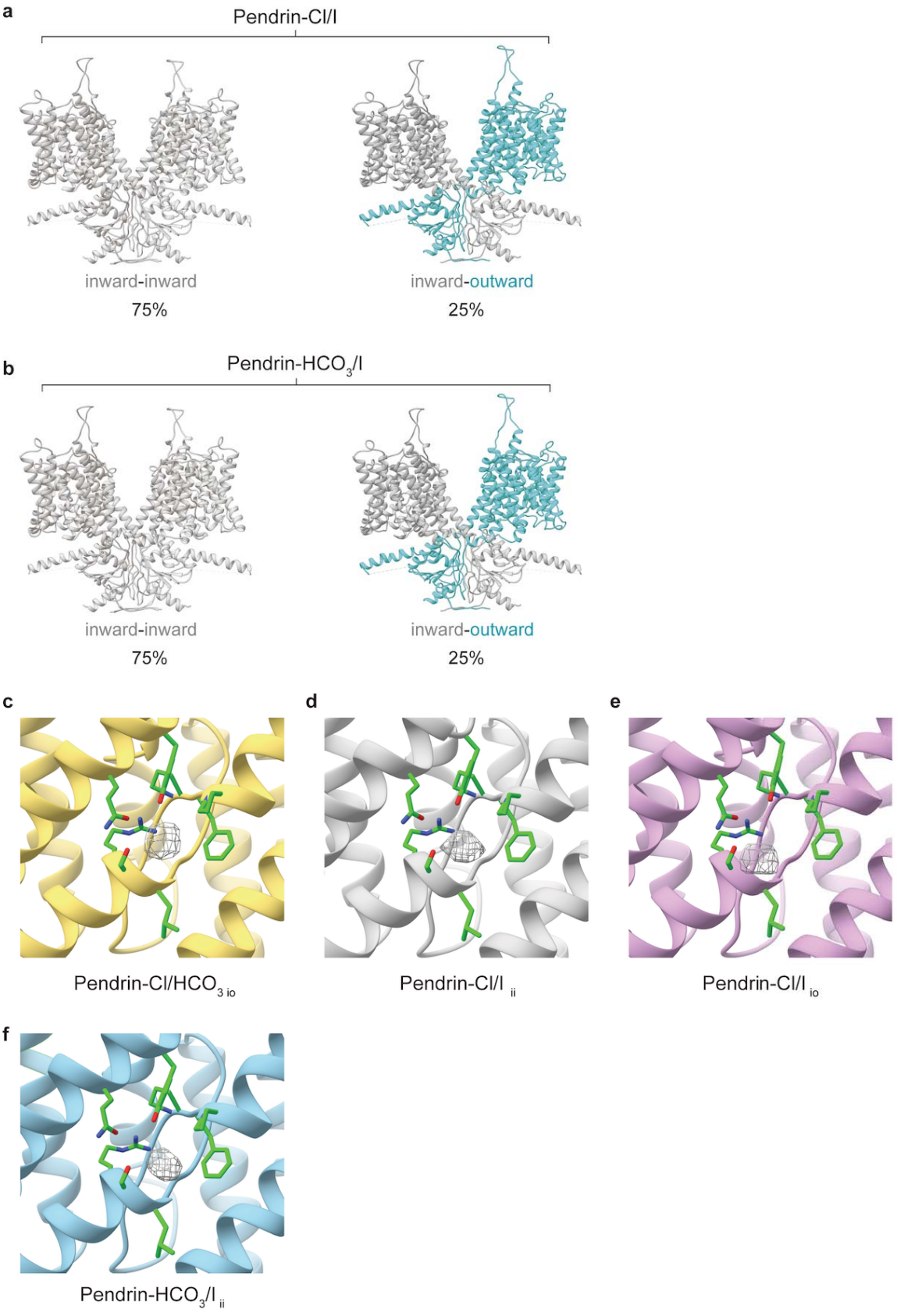
a
Pendrin-Cl/I
inward-inward
75%
inward-outward
25%
b
Pendrin-HCO3/I
inward-inward
75%
inward-outward
25%
c
Pendrin-Cl/HCO3 io
d
Pendrin-Cl/I ii
e
Pendrin-Cl/I io
f
Pendrin-HCO3/I ii

Supplementary Fig. 3 Conformations of pendrin-Cl/I and pendrin-HCO_3/I and anion densities we observed in the inward-open pocket of these structures.

a and b, Two conformations of pendrin-Cl/I and pendrin-HCO_3/I. The proportion of particles is indicated. **c-f,** Besides the pendrin-Cl and pendrin-HCO_3 in the main figure, the anion densities we absorbed in the inward-open pocket of the rest structures, c shows pendrin-Cl/$HCO_{3\ io}$, d shows pendrin-Cl/I_{ii}, e shows pendrin-Cl/I_{io} and f shows pendrin-HCO_3/I_{ii}. ii: inward-inward, io: inward-outward, oo: outward-outward for protomer A and protomer B, respectively. Density is shown in the light grey mesh.

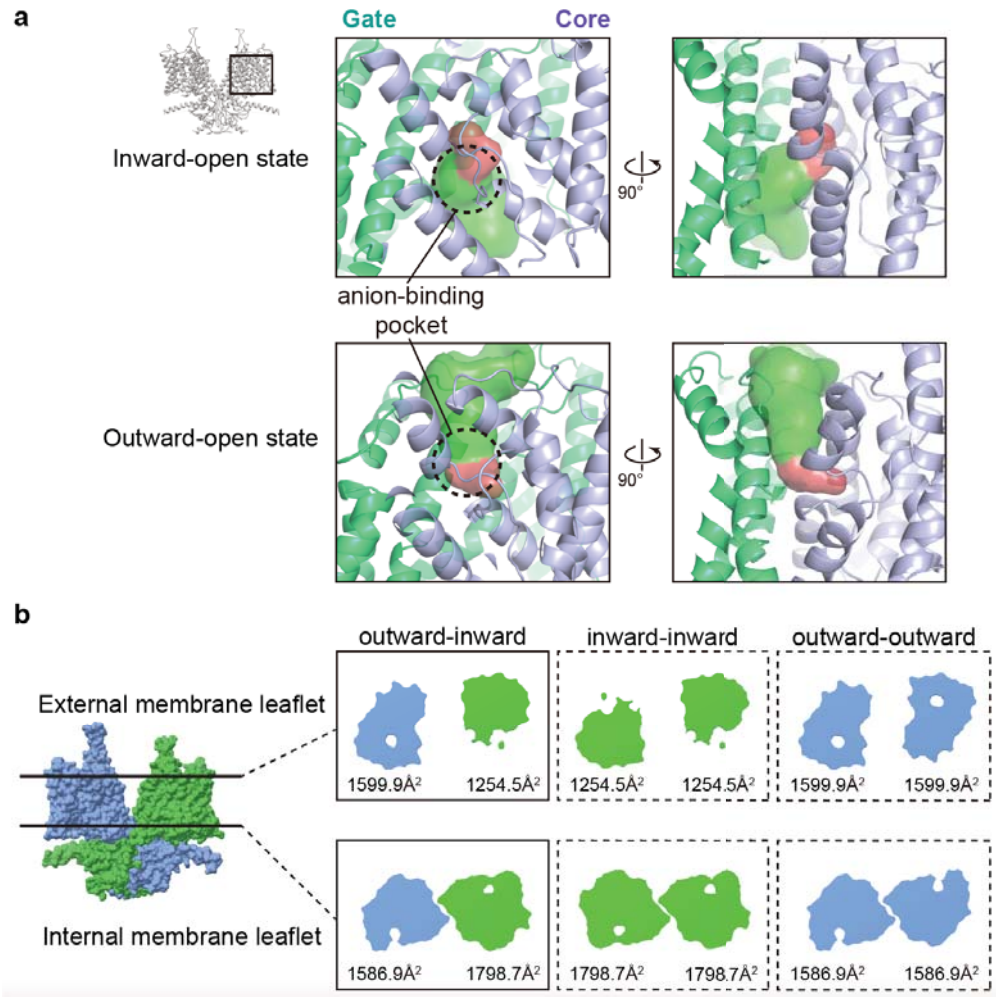

Supplementary Fig. 4 Anion pathway cavity and cross-section area of the inward-open state and the outward-open state TMDs.

Anion pathway analyzed by HOLE. Because pendrin functions in the manner of alternative accessing, we analyzed the inward-open TMD and outward-open TMD, respectively. **a,** The cavities from the anion-binding pocket to the intracellular or extracellular space (red cavity indicates the pathway diameter smaller than 3 Å, and green cavity indicates the pathway diameter larger than 3 Å). **b,** At the outer leaflet and the inner leaflet, cross-section areas of pendrin in three conformations are shown.

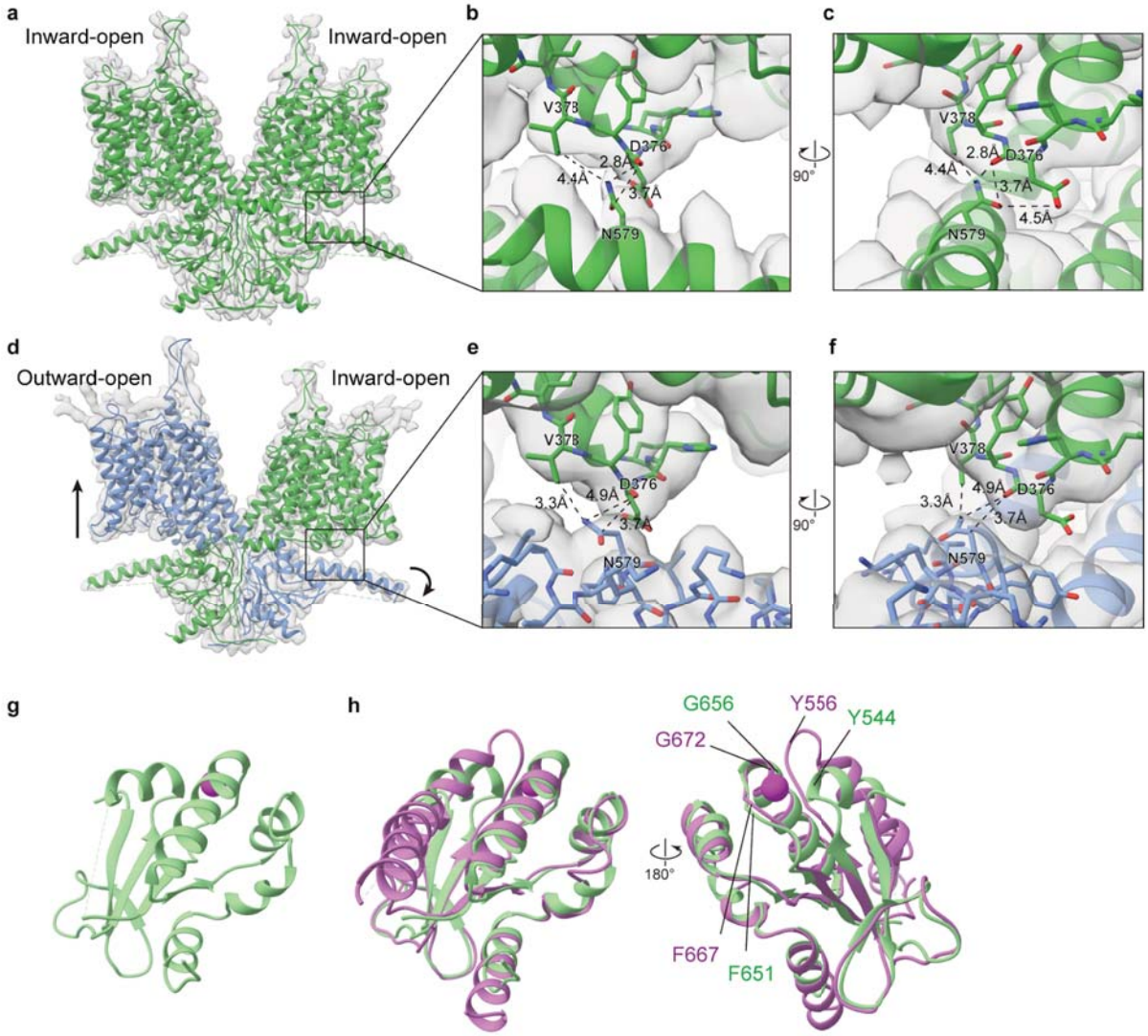

Supplementary Fig. 5 Details of the interaction between STAS domain helix Cα1b and TMD and "pre-binding site".

a-c, In inward-open state C2 structures, the helix Cα1b is the most close to the TMD (N579 of helix Cα1b interacts with D376 of TM8 in core region). **d-f,** In the outward-open protomer of the asymmetric structures, the helix Cα1b rotates about 6° away and the core moves up to the extracellular space (marked by black arrows). Therefore, below the inward-open TMD, N579 gets a little away from D376 by Cα1b rotation. And below the outward-open TMD, interaction is broken by core's movement. **g,** Crystal structure of rat prestin STAS domain in complex with chloride (PDBID: 5EUU). A Cl^- in the pre-binding site is shown in magenta. **h,** Comparison of rat prestin STAS domain (light green) with pendrin STAS domain (orchid). F667, G672 and Y556 of pendrin are labeled.

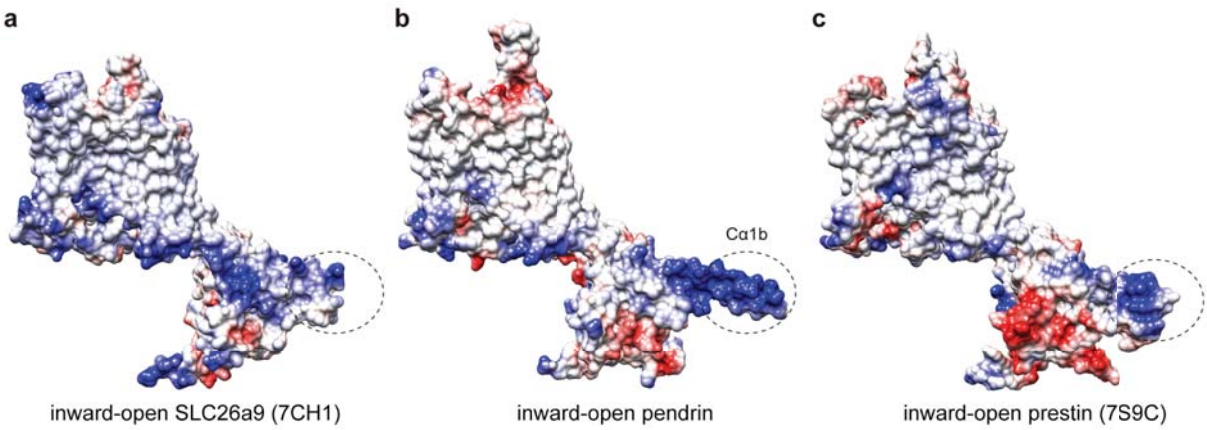

Supplementary Fig. 6 a-c, Electrostatic potential surface of pendrin, prestin, and SLC26a9 protomers, showing the positive surface charge of Cα1b.

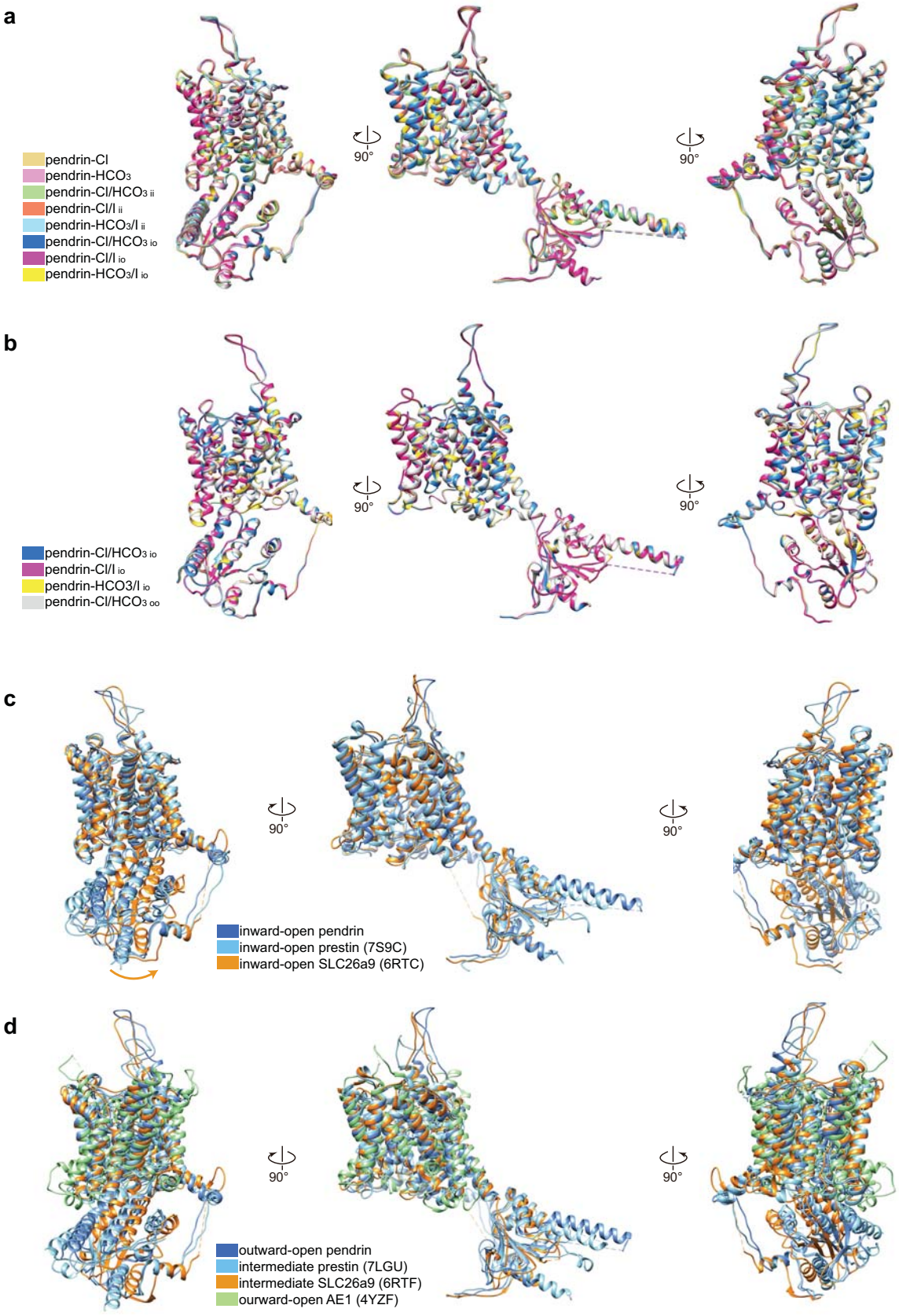
a
pendrin-Cl
pendrin-HCO3
pendrin-Cl/HCO3 ii
pendrin-Cl/I ii
pendrin-HCO3/I ii
pendrin-Cl/HCO3 io
pendrin-Cl/I io
pendrin-HCO3/I io
90°
90°
b
pendrin-Cl/HCO3 io
pendrin-Cl/I io
pendrin-HCO3/I io
pendrin-Cl/HCO3 oo
90°
90°
c
inward-open pendrin
inward-open prestin (7S9C)
inward-open SLC26a9 (6RTC)
90°
90°
d
outward-open pendrin
intermediate prestin (7LGU)
intermediate SLC26a9 (6RTF)
ourward-open AE1 (4YZF)
90°
90°

Supplementary Fig. 7 Structural comparison of pendrin, prestin, SLC26A9, and AE1.

a, Superimposing the inward-open protomers among 8 pendrin structures (pendrin-Cl, pendrin-HCO_3, pendrin pendrin-Cl/$HCO_{3\ ii}$, pendrin-Cl/I_{ii}, pendrin-HCO_3/I_{ii}, pendrin-Cl/$HCO_{3\ io}$ chain A, pendrin-Cl/I_{io} chain A, pendrin-HCO_3/I_{io} chain A). RMSDs are listed in Supplementary Table 1. **b,** Superimposing the outward-open protomers among 4 pendrin structures (pendrin-Cl/$HCO_{3\ io}$ chain B, pendrin-Cl/I_{io} chain B, pendrin-HCO_3/I_{io} chain B, pendrin-Cl/$HCO_{3\ oo}$). RMSDs are listed in Supplementary Table 1. **c,** Superimposing the inward-open protomers of pendrin-Cl, prestin (PDBID: 7S9C), SLC26A9 (PDBID: 6RTC). RMSDs are listed in Supplementary Table 2. **d,** Superimposing the outward-open protomers of pendrin-Cl/$HCO_{3\ oo}$, prestin (PDBID: 7LGU), SLC26A9 (PDBID: 6RTF), TMD of AE1 (PDBID: 4YZF). RMSDs are listed in Supplementary Table 2.

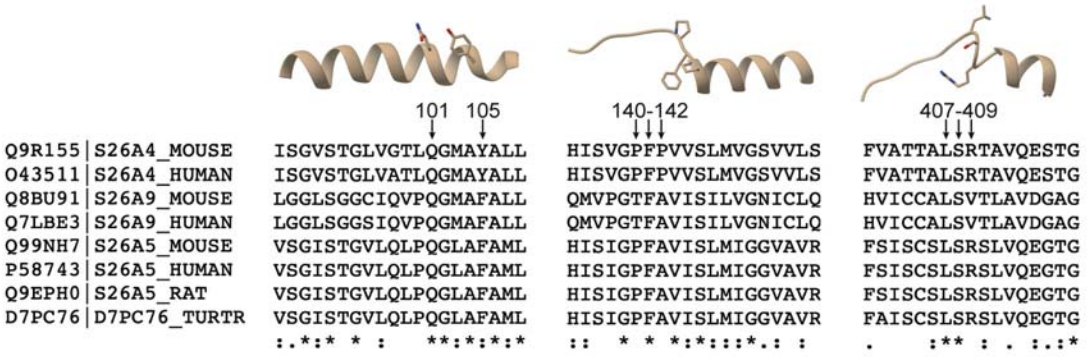

Supplementary Fig. 8 SLC26A homologs sequence alignment around the anion binding pocket.

These sequences were obtained from UniProt. The entry identifier is listed along with the protein name on the left.

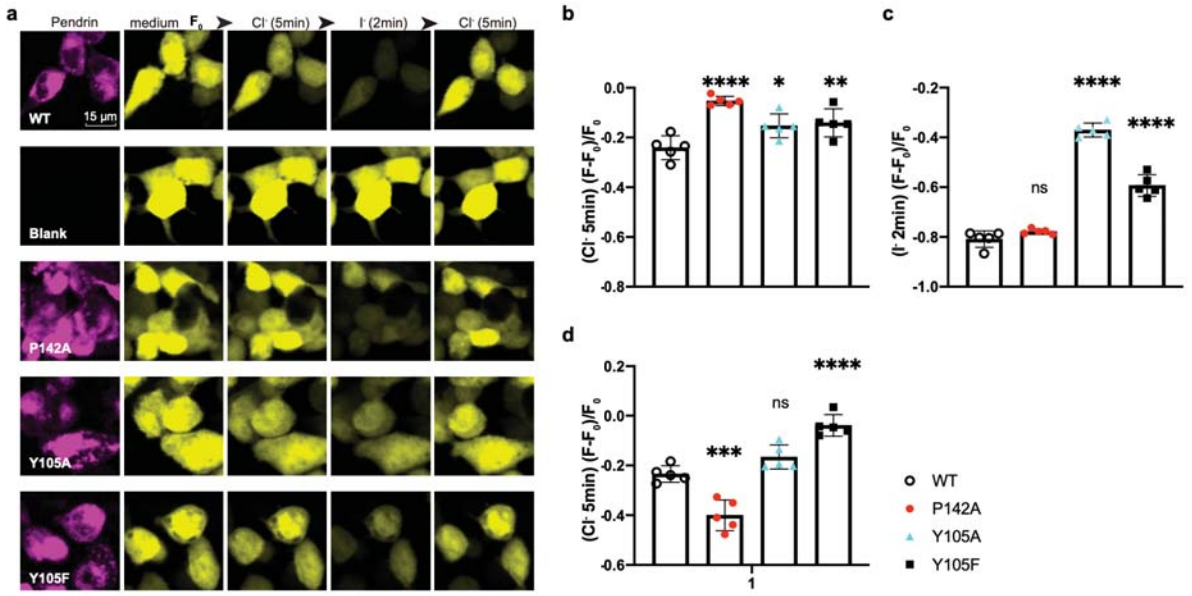

e

	Dunnett's multiple comparisons test	Mean Diff.	95.00% CI of diff.	Adjusted P Value
Cl^- 5min	WT vs. P142A	-0.188	-0.2621 to -0.1139	<0.0001
	WT vs. Y105A	-0.08795	-0.1621 to -0.01384	0.019
	WT vs. Y105F	-0.1001	-0.1742 to -0.02601	0.0079
I^- 2 min	WT vs. P142A	-0.03049	-0.08163 to 0.02064	0.314
	WT vs. Y105A	-0.4386	-0.4898 to -0.3875	<0.0001
	WT vs. Y105F	-0.2158	-0.2670 to -0.1647	<0.0001
Cl^- 5 min	WT vs. P142A	0.166	0.08747 to 0.2446	0.0002
	WT vs. Y105A	-0.06853	-0.1471 to 0.01004	0.0937
	WT vs. Y105F	-0.1954	-0.2739 to -0.1168	<0.0001

Supplementary Fig. 9 Fluorescence change of HEK293T cells in Cl^-/I^- exchange assay.
a, Enlargement of raw fluorescence micrographs. **b-d,** At three time points, One-way ANOVA with Dunnett's multiple comparison test was performed for comparison between multiple groups. n= 5 cells examined over 3 independent experiments. Data are presented as mean values, error bars indicate SD. Multiple comparison results were the comparison versus the cells transfected with WT pendrin, ****P < 0.0001, ***P < 0.001, **P < 0.01, and *P < 0.05. **e.** Details of Dunnett's multiple comparisons test.

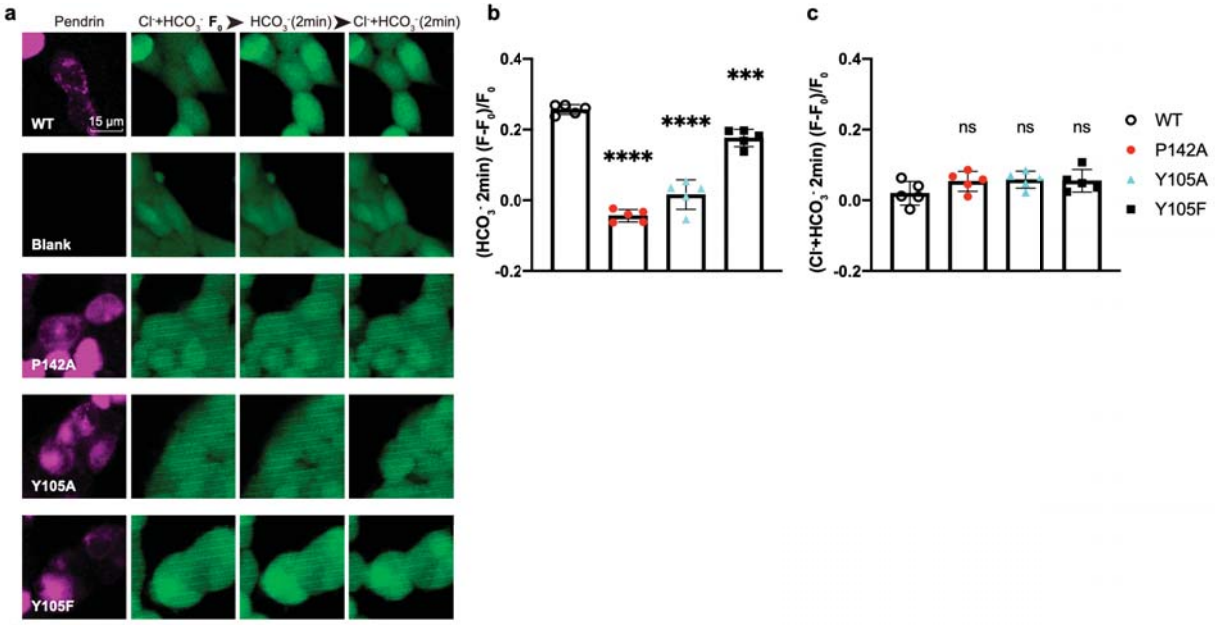

d

	Dunnett's multiple comparisons test	Mean Diff.	95.00% CI of diff.	Adjusted P Value
HCO_3^- 2min	WT vs. P142A	0.3006	0.2568 to 0.3444	<0.0001
	WT vs. Y105A	0.2407	0.1968 to 0.2845	<0.0001
	WT vs. Y105F	0.08033	0.03650 to 0.1242	0.0006
$Cl^-+HCO_3^-$ 2min	WT vs. P142A	-0.03364	-0.08223 to 0.01494	0.2121
	WT vs. Y105A	-0.03836	-0.08695 to 0.01022	0.1381
	WT vs. Y105F	-0.03473	-0.08331 to 0.01385	0.1927

Supplementary Fig. 10 Fluorescence change of HEK293T cells in Cl^-/HCO_3^- exchange assay. **a,** Enlargement of raw fluorescence micrographs. **b-c,** At two time points, One-way ANOVA with Dunnett's multiple comparison test was performed for comparison between multiple groups. n= 5 cells examined over 3 independent experiments. Data are presented as mean values, error bars indicate SD. Multiple comparison results were the comparison versus the cells transfected with WT pendrin, ****P < 0.0001, ***P < 0.001, **P < 0.01, and *P < 0.05. **d.** Details of Dunnett's multiple comparisons test.

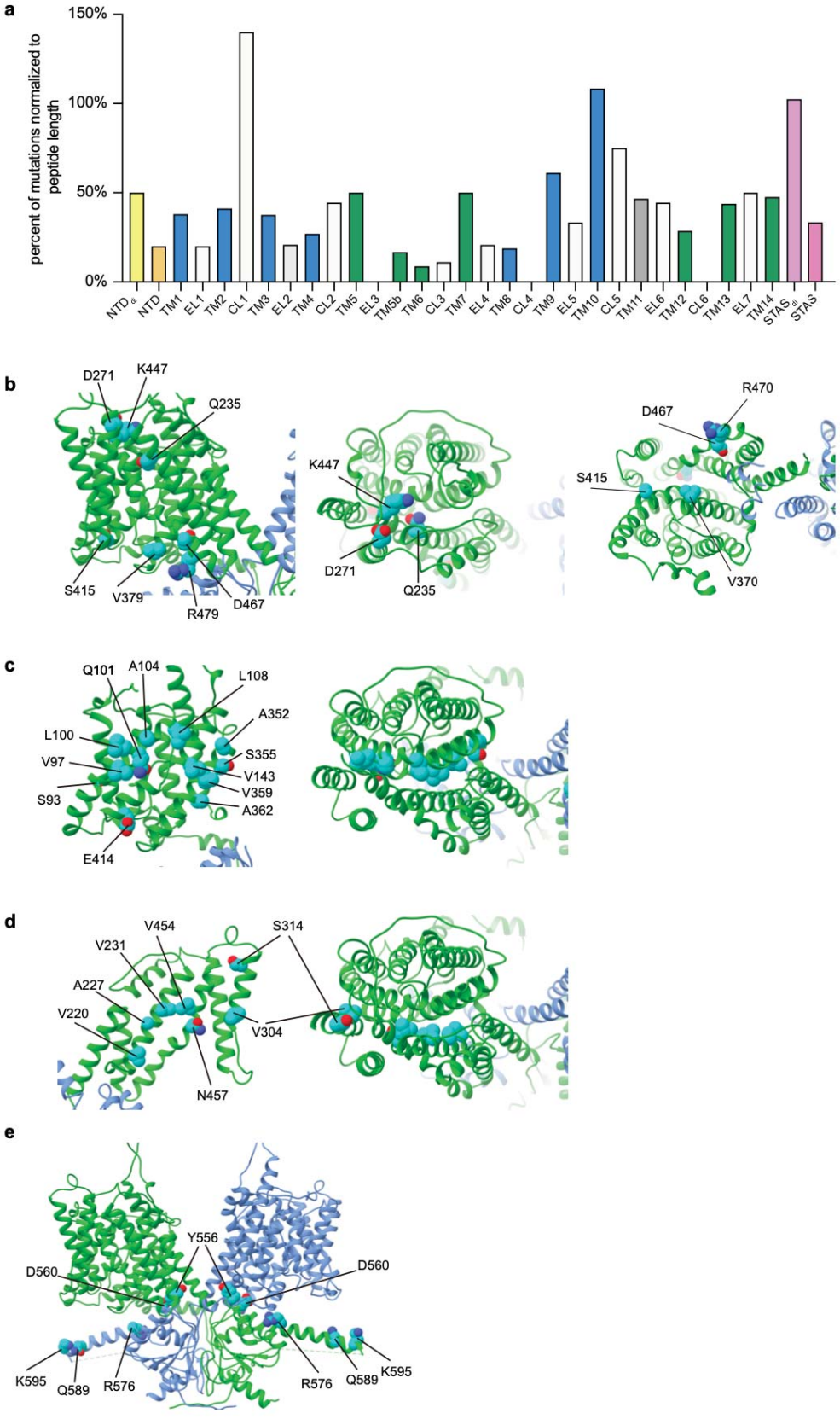
a
150%
100%
50%
0%
percent of mutations normalized to peptide length
NTDα
NTD
TM1
EL1
TM2
CL1
TM3
EL2
TM4
CL2
TM5
EL3
TM5b
TM6
CL3
TM7
EL4
TM8
CL4
TM9
EL5
TM10
CL5
TM11
EL6
TM12
CL6
TM13
EL7
TM14
STASα
STAS
b
D271
K447
Q235
S415
V379
R479
D467
K447
D271
Q235
R470
D467
S415
V370
c
Q101
A104
L108
A352
L100
S355
V97
V143
V359
S93
A362
E414
d
V454
S314
V231
A227
V220
V304
N457
e
Y556
D560
D560
K595
Q589
R576
R576
Q589
K595

Supplementary Fig. 11 Summary of 261 pathogenetic mutations of pendrin.

a, Based on the deafness variation database (https://deafnessvariationdatabase.org; accessed on 20 Sep 2022), 261 of 761 missense disease-associated mutations are pathogenetic in clinic. NTD_{di} indicates the residue in the dimerization interface of NTD, EL indicates the extracellular loop, CL indicates the cytosolic loop, and $STAS_{di}$ indicates the residue in the dimerization interface of STAS. **b,** Mutations along the anion exchange pathway that would change local charge. **c,** In the core region, mutation locations happened to change the interface profile. **d,** In the gate region, mutations are located on the core-gate interface regions. **e,** On the positively charged platform, the mutation locations happened to change charge.

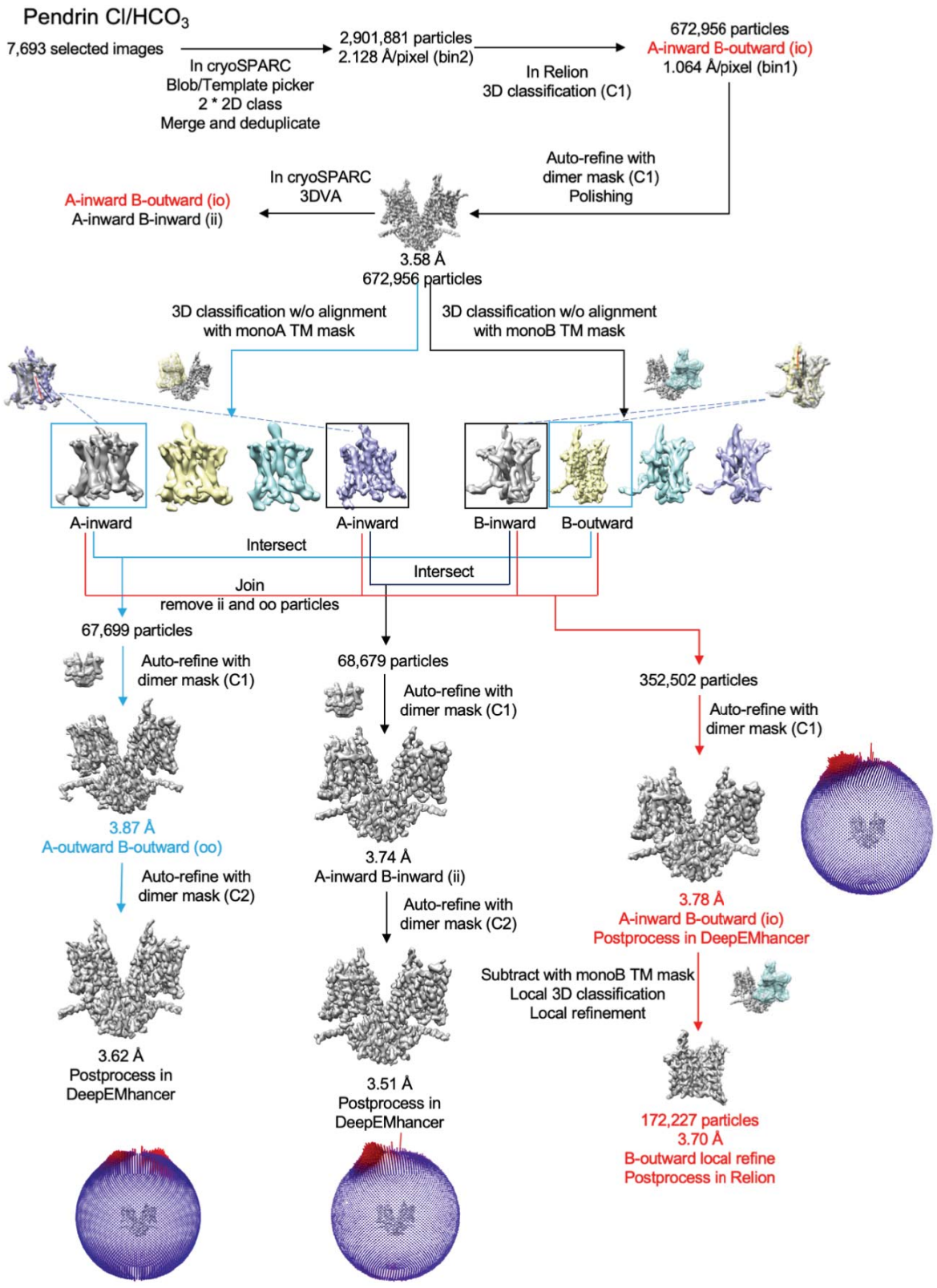

Supplementary Fig. 12 Flowchart of pendrin-Cl/HCO_3 data processing.

Supplementary Table 1 Comparison of pendrin structures at different conditions (RMSD).

pendrin-Cl												
Pendrin-HCO_3	0.3 (Å)											
pendrin-$Cl/HCO_{3\ ii}$	0.4	0.4										
pendrin-Cl/I_{ii}	0.4	0.4	0.4									
pendrin-HCO_3/I_{ii}	0.4	0.4	0.4	0.3								
pendrin-$Cl/HCO_{3\ io}$ A	0.5	0.5	0.4	0.5	0.5							
pendrin-$Cl/HCO_{3\ io}$ B	4.4	4.5	4.4	4.4	4.4	4.4						
pendrin-Cl/I_{io} A	0.5	0.5	0.4	0.4	0.5	0.2	4.3					
pendrin-Cl/I_{io} B	4.4	4.5	4.3	4.3	4.3	4.3	0.2	4.3				
pendrin-HCO_3/I_{io} A	0.5	0.5	0.5	0.5	0.5	0.2	4.4	0.3	4.4			
pendrin-HCO_3/I_{io} B	4.3	4.4	4.3	4.3	4.3	4.3	0.2	4.3	0.2	4.4		
pendrin-$Cl/HCO_{3\ oo}$	4.5	4.6	4.4	4.4	4.5	4.4	0.3	4.4	0.4	4.5	0.4	
	pendrin-Cl	pendrin-HCO_3	pendrin-$Cl/HCO_{3\ ii}$	pendrin-Cl/I_{ii}	pendrin-HCO_3/I_{ii}	pendrin-$Cl/HCO_{3\ io}$ A	pendrin-$Cl/HCO_{3\ io}$ B	pendrin-Cl/I_{io} A	pendrin-Cl/I_{io} B	pendrin-HCO_3/I_{io} A	pendrin-HCO_3/I_{io} B	pendrin-$Cl/HCO_{3\ oo}$

Supplementary Table 2 Comparison of pendrin structures with representative structures of prestin and SLC26A9 (RMSD).

Pendrin-Cl										
SLC26A9 (6RTC)	4.6 (Å)									
SLC26A9 (7CH1)	4.1	3.4								
Prestin (7S9C)	3	5.3	5.3							
Prestin (7LH2)	3.8	6.3	6.3	2.3						
Prestin (7S9D)	3.1	6.1	6	2.1	1.9					
Prestin (7S8X)	3.6	6.9	7.2	2.7	1.6	1.9				
Prestin (7LGU)	4.5	7.5	8	3.1	1.2	2.4	1.4			
SLC26A9 (6RTF)	4.3	3	4.8	4.3	4.4	4.8	5.1	5.8		
Pendrin-$Cl/HCO_{3\ oo}$	4.5	7	6.8	4.4	4.2	3.8	3.3	3.9	5.1	
	Pendrin-Cl	SLC26A9(6RTC)	SLC26A9(7CH1)	Prestin (7S9C)	Prestin (7LH2)	Prestin (7S9D)	Prestin (7S8X)	Prestin (7LGU)	SLC26A9(6RTF))	Pendrin-$Cl/HCO_{3\ oo}$

Supplementary Table 3 Cryo-EM data collection and refinement statistics.

	pendrin-Cl	pendrin-HCO_3	pendrin-Cl/I_{ii}	pendrin-Cl/I_{io}	pendrin-Cl/$HCO_{3\ ii}$	pendrin-Cl/$HCO_{3\ io}$	Local refinement of pendrin-Cl/$HCO_{3\ io}$	pendrin-Cl/$HCO_{3\ oo}$	pendrin-HCO_3/I_{ii}	pendrin-HCO_3/I_{io}
PDB ID	7WK1	7WK7	7WL8	7WLB	7WL7	7WL9		7WLE	7WL2	7WLA
EMDB	32555	32561	32577	32580	32576	32578	33232	32583	32574	32579
Data collection and processing										
Data sets	pendrin-Cl	pendrin-HCO_3	pendrin-Cl/I			pendrin-Cl/HCO_3			pendrin- HCO_3/I	
Voltage (kV)	300	300	300			300			300	
Detector	K2	K2	K3			K3			K2	
Pixel size (Å)	1.046	1.046	1.064			1.064			1.046	
Electron dose (e^-/Å^2)	53	53	58			58			53	
Defocus range (μm)	−1.2 to −2.2	−1.2 to −2.2	−1.2 to −2.2			−1.2 to −2.2			−1.2 to −2.2	
Final particles	120,887	134,404	79,043	45,859	68,679	353,288	172,227	67,699	221,446	365,679
Final resolution (Å)	3.25	3.49	3.40	4.10	3.51	3.78	3.70	3.62	3.25	3.76
Model refinement and validation statistics										
Ramachandran statistics										
Favored (%)	94.70	94.93	95.31	95.45	95.31	95.30		93.92	95.01	94.92
Allowed (%)	5.22	4.99	4.61	4.55	4.61	4.62		6.08	4.92	5.08
Outliers (%)	0.08	0.08	0.08	0.00	0.08	0.08		0.00	0.08	0.00
Rotamer outliers (%)	3.12	2.94	1.87	3.92	3.39	4.27		5.25	2.14	4.01
R.m.s.deviations										
Bond lengths (Å)	0.002	0.001	0.002	0.002	0.001	0.002		0.002	0.002	0.002
Bond angles (°)	0.406	0.406	0.402	0.400	0.409	0.403		0.426	0.412	0.405